A Multi-objective Group Sparse Hyperspectral Unmixing Method with High Correlation Library

Yanyi Wei, Xia Xu, Bin Pan, Tao Li and Zhenwei Shi

Abstract

Hyperspectral sparse unmixing aims at modeling pixels of hyperspectral image as linear combination of a subset of a prior spectral library. Over the past years, spectral library has been constantly expanded, including spectra of the same material with intrinsic variability, which may result in the problem of high correlation. Recently, multi-objective sparse unmixing methods presented promising performance in dealing with sparsity via a non-convex $\mathcal{L}_0$ norm, but are insensitive to identifying endmembers with high correlation. In this paper, we propose a multi-objective sparse unmixing method, multi-objective group sparse hyperspectral unmixing (MO-GSU), which integrates a group sparsity structure to address high correlation of the spectral library induced by spectral variability. In order to describe the sparsity within and among groups, MO-GSU develops a mixed norm $\mathcal{L}_{0,q}$ instead of the $\mathcal{L}_0$ norm. During the optimization, we propose two new search strategies: intra-group local search and group oriented adaptive genetic operator. The intra-group local search strategy is presented in addition to the multi-objective evolutionary algorithm for better exploitation within groups. The group oriented adaptive genetic operator is designed to maintain the inter-group distribution between generations and further ensure the intra-group exploitation. Moreover, we provide theoretical proof for the advantage of the group operators in exploiting the endmembers within group. To verify the efficiency of the proposed method on high correlation situations, MO-GSU is compared with recently proposed endmember bundle based and multi-objective based sparse unmixing methods on synthetic and real data with high correlation libraries.

Index Terms

Hyperspectral unmixing, Multi-objective optimization, Group sparsity.

I. INTRODUCTION

Hyperspectral image (HSI) is a three-dimensional data cube containing abundant spectral information in the form of reflectance of numerous continuous spectral bands. Spectral signatures vary from material to material due to the high spectral resolution of hyperspectral sensors, allowing precise identification of materials from an image. Informative as an HSI be on the spectral dimension, the spatial resolution of hyperspectral sensors suffers to be relatively low [1]. As a result, there exists mixed pixel, as in one pixel containing multiple materials. In recent years, many hyperspectral unmixing techniques have been developed to identify pure material signatures (called *endmembers*) in each pixel of the HSI, and estimate their proportions (called *abundances*) at the same time [2]–[4].

Linear mixture model is a popular description of the unmixing process. Unlike nonlinear models which takes account of multiple reflectance and scattering from various materials [5], [6], linear mixture model assumes the signature of a pixel to be a linear combination of spectra signatures of pure materials. Different approaches have been addressed under the assumption of linear mixture model in the past decades, including categories of geometrical approaches, statistical approaches, non-negative matrix factorization and sparse regression approaches [4], [7]. Geometrical approaches consider the linearly mixed signatures with the sum-to-one constraint on abundances in a simplex, of which the vertices represent the endmembers and the volume is the optimization objective [8]–[10]. Statistical approaches such as bayesian methods perform bayesian inference and parameter estimation on endmembers and abundances [11], [12]. Non-negative matrix factorization resolves the observed image into endmember and abundance matrices [13]–[15]. Sparse regression approaches exploit a redundant prior spectral library as endmember candidates, assuming the observed image a linear combination of pure spectra signatures from a subset of the spectral library [16]. Sparse unmixing is a semi-supervised approach including endmember selection and abundance inversion procedures, thus has no need for pure pixel assumptions. The method proposed in this paper is a sparse unmixing approach.

Nevertheless, sparse unmixing expects the challenge of how to optimize the sparsity of endmembers directly expressed via $\mathcal{L}_0$ norm. The $\mathcal{L}_0$ norm regularization formulates a nonconvex and NP-hard optimization objective. Convex approximation and greedy search are the two common solution to address $\mathcal{L}_0$ norm. Literature [17] converted the nonconvex problem into a convex form by proposing SUnSAL to relax $\mathcal{L}_0$ norm into $\mathcal{L}_1$ norm. Literature [18] adopted $\mathcal{L}_{0,\frac{1}{2}}$ quasinorm, a better approximation of $\mathcal{L}_0$ norm as penalty and an iterative algorithm for abundance estimation. Literature [19] designed a numerical reweighted least squares algorithm for the constrained sparse l_p-l_2 $(0 < p < 1)$ optimization problem. Literature [8] employs sparsity criteria based library pruning and explores standard sparsity measures such as Gini index and pd-norm sparsity. The boosting deep learning methods have provided promising results on many image processing tasks, and literature [20] proposes SUnCNN, a deep convolutional encoder–decoder, to solve sparse unmixing problem.

Multi-objective optimization is an effective solution for overcoming the difficulty induced by the nonconvex optimization [21]. Sparse unmixing task is naturally a bi-objective problem as simultaneously minimizing the reconstruction error of image data and endmember sparsity applied with $\mathcal{L}_0$ norm. The $\mathcal{L}_0$ norm sparsity determines multi-objective sparse unmixing to be an NP-hard problem. Multi-objective evolutionary algorithms (MOEAs) are

proved to be available and effective for NP-hard problems. Many multi-objective sparse unmixing algorithms have arisen in recent years [22]–[26]. MOSU [27] translated sparse unmixing into a tri-objective problem and employs a cooperative coevolutionary strategy. SMOSU [28] regarded sparse unmixing as a bi-objective problem, applying binary decision vector and a random flipping strategy. PMOSU [29] simultaneously performed library pruning and sparse regression through a gradual compression of search space. Jiang [30] proposed an improved two phase approach with extra application of spatial-contextual information.

However, the classic multi-objective sparse unmixing methods may suffer the problem of inadequate searching performance due to the high correlation of the spectral library caused by spectral variability. Spectral variability enlarges the scale of prior spectral library and raises correlation. The inadequate search is an inevitable outcome since the classic MOEAs are not capable of simulating the Pareto Front within bearable evaluations when confronting large-scale multi-objective problems [31]. The spectral variability effect [32], namely several spectral signatures representing one single material, occurs attributed to the variation of intrinsic property and extrinsic conditions such as illumination and atmosphere. Methods addressing spectral variability can be divided into two main categories. On the one hand, researchers adjust the conventional LMM model to cover the variation of extrinsic conditions [33], [34]. On the other hand, intrinsic variation is expressed via multiple detected instances of one particular material, called endmember bundles [35]–[37]. Literature [38] extracted endmember bundles to construct spectral library with high correlation, and adopted a mixed norm for class and intra-class sparsity. Dictionary pruning methods eliminate correlation by reducing mutual coherence [39]. Literature [40] presented a recursive PCA approach as well as a mutual coherence reduction method for library pruning.

In this paper, we propose a new multi-objective group sparse unmixing algorithm MO-GSU to address high correlation within endmember bundles in the spectral library. There are threefold strategies presented to tackle with high correlation caused by spectral variability and the resultant group structure formed of endmember bundles. 1) In order to interpret the sparsity within and among groups, we introduce a mixed norm $\mathcal{L}_{0,q}$ in MO-GSU containing group structure information, where q is a real value between 0 and 1, still formulating an NP-hard problem. The sparsity of material and each endmember underlies in the inherent requirement of hyperspectral unmixing. The proposed MO-GSU tailored for spectral libraries with correlation is then used to optimize the bi-objective problem. 2) An intra-group local search strategy is presented in addition to the multi-objective evolutionary algorithm to exploit endmember selection within certain groups [41]–[43], significantly improving the effectiveness and efficiency of endmember selection. 3) Furthermore, to balance exploitation and exploration, this paper employs a group oriented adaptive genetic operator, including a crossover operator involving group structure to maintain the distribution within group between generations during the evolutionary process, and an intra-group mutation operator to further ensure the intra-group exploitation.

The contributions of MO-GSU include the following aspects:

1) We propose an advanced multi-objective hyperspectral unmixing method for a mixed $\mathcal{L}_{0,q}$ norm model based on group sparsity, which aims at addressing the high correlation of spectral library.

2) In the proposed MOEA, we design two group based optimization strategies, intra-group local search and group oriented adaptive genetic operator, to enhance intra-group exploitation and inter-group exploration.

3) We further provide theoretical proof for the proposed genetic operator of a more sufficient endmember exploitation within group.

II. Proposed Method

In this section, we first introduce some background context on unmixing model, group sparsity with mixed norm and multi-objective evolutionary algorithms. Then, we elaborate on the proposed multi-objective group sparse unmixing method. To start with, we demonstrate the mathematical expression of the group sparse unmixing problem and the framework of the proposed MO-GSU method. In section II-A, we first introduce some background context. Section II-B presents the model of MO-GSU. Section II-C describes the optimization process, and we detail the techniques aimed at intra-group correlation orderly in section II-D and II-E.

A. Background

1) LMM: Linear mixing model (LMM) assumes each pixel in an HSI as a linear combination of pure spectral signatures:

$$\mathbf{y}_i = \mathbf{A}\mathbf{x}_i + \mathbf{n}_i, \tag{1}$$

where $\mathbf{y}_i \in \mathbb{R}^{L \times 1}$ is the reflectance vector of the i-th pixel from an observed image over L spectral bands, $\mathbf{A} \in \mathbb{R}^{L \times m}$ is the spectral signature matrix associated with m endmembers, $\mathbf{x}_i \in \mathbb{R}^{m \times 1}$ is the corresponding abundance vector of the m endmembers, and $\mathbf{n}_i \in \mathbb{R}^{L \times 1}$ is a vector collecting noise and modeling error. Equation (1) can be rewritten considering n pixels in the observed image in Equation (2):

$$\mathbf{Y} = \mathbf{A}\mathbf{X} + \mathbf{N}, \tag{2}$$

where $\mathbf{Y} = [\mathbf{y}_1, \mathbf{y}_2, \ldots, \mathbf{y}_n] \in \mathbb{R}^{L \times n}$ denotes the reflectance matrix of the whole image, $\mathbf{X} \in \mathbb{R}^{m \times n}$ denotes the abundances of m endmembers on n pixels, and $\mathbf{N} \in \mathbb{R}^{L \times n}$ represents the noise matrix. The abundance of each pixel satisfies the abundance nonnegative constraint (ANC): $x_{ij} \geq 0, j = 1, 2, \ldots, n$ and the abundance sum-to-one constraint (ASC): $\sum_{i=1}^{m} x_{ij} = 1, j = 1, 2, ..., n$. In this paper, nonnegative constrained least square method is adopted to inverse the abundance matrix after endmember selection.

2) Endmember Bundles and Mixed Norm: Sparse unmixing methods utilize a prior spectral library as endmember candidates and implement constrained least square regression on the optimal subset for abundance inversion. The prior library which can be represented as $\mathbf{A}$ in Equation (2) is designed to adapt to various image scenes. To this end, the library is supposed to be redundant, as in sparsity of nonzero rows of $\mathbf{A}$ in Equation (2). The conventional sparse unmixing task is expressed as Equation (3).

$$\min_{\mathbf{X}} \| \mathbf{X} \|_{\text{row}-0},$$
$$\text{s.t. } \| \mathbf{Y} - \mathbf{A}\mathbf{X} \|_{\text{F}} \leq \delta, \mathbf{X} \geq 0. \tag{3}$$

where δ is the tolerance of reconstruction value, $\| \cdot \|_{\text{row}-0}$ and $\| \cdot \|_{\text{F}}$ denote the numbers of nonzero rows and the Frobenius norm of a matrix.

However, Equation (3) does not exploit the grouping information of the prior library. Due to the spectral variation of extrinsic and intrinsic properties, it is common in a spectral library that several spectra represents single material. Therefore, different realizations of the same material compose endmember bundles, and the intrinsic similarity within bundles formulates certain group structure. Given such additional group structure G, the $\mathcal{L}_0$-norm sparsity is translated into group sparsity in $\mathcal{L}_{G,p,q}$ norm, $0 < p, q < 1$. The sparse unmixing task containing grouping information is expressed via Equation (4).

$$
\begin{aligned}
&\min_{\mathbf{X}} \parallel \mathbf{X} \parallel_{G,p,q}, \\
&\text{s.t. } \parallel \mathbf{Y} - \sum_{g=1}^{|G|} \mathbf{A}_g \mathbf{X}_g \parallel_{\mathrm{F}} \leq \delta, \mathbf{X} \geq 0.
\end{aligned}
\tag{4}
$$

where G denotes the grouping strategy, $\mid G \mid$ is the number of groups, $\mathbf{A}_g$, $\mathbf{X}_g$ are the corresponding grouping endmembers and abundance of indices from group g respectively, and $\parallel \cdot \parallel_{G,p,q}$ denotes the mixed norm of a matrix, $0 < p, q < 1$. The $\mathcal{L}_{G,p,q}$ norm of a vector $\mathbf{x}$ and group structure G is defined in Equation (5) for any real p, q, where $\mid G_i \mid$ denotes the size of the i-th group.

$$
\parallel \mathbf{x} \parallel_{G,p,q} = \left(\sum_{i=1}^{|G|} \left(\sum_{j=1}^{|G_i|} \mid \mathbf{x}_{G_i,j} \mid^p \right)^{\frac{q}{p}} \right)^{\frac{1}{q}} = \left(\sum_{i=1}^{|G|} \parallel \mathbf{x}_{G_i} \parallel_p^q \right)^{\frac{1}{q}}
\tag{5}
$$

When $(p, q) = (0, 1)$, the group sparsity is reduced to $\mathcal{L}_0$-norm in Equation (3). The group sparsity with (p, q) values of $(1, 1), (2, 1), (1, 2), (1, q), 0 < q < 1$, correspond to regular lasso, group lasso, elitist lasso, and fractional lasso respectively. In this article, we set $(p, q) = (0, q)$, $0 < q < 1$, thus adopting group sparsity of $\mathcal{L}_{G,0,q}$ norm, since it's a better reflection of both inter-group and intra-group sparsity than the regular $\mathcal{L}_0$-norm.

3) Multi-objective Optimization: A minimization multi-objective problem (MOP) of k objectives can be presented as follow:

$$
\begin{aligned}
&\min_{\mathbf{s}} F(\mathbf{s}) = [f_1(\mathbf{s}), f_2(\mathbf{s}), \ldots, f_k(\mathbf{s})]^T \\
&\text{s.t. } h_i(\mathbf{s}) \leq 0, i = 1, 2, \ldots, c_1, \\
&h_j(\mathbf{s}) = 0, j = 1, 2, \ldots, c_2.
\end{aligned}
\tag{6}
$$

where $\mathbf{s}$ is a feasible solution in the decision space Ω, which is established by inequality and equality constraints $h_i(\mathbf{s})$ and $h_j(\mathbf{s})$.

MOPs aim at simultaneously optimizing more than one objective function which conflict with each other for most cases. Therefore, the trade-off relation among objectives is in consideration and a criterion assessing multiple objectives is in need. To this end, the concept of Pareto dominance is introduced as follow. For two feasible solutions $\mathbf{s}_1, \mathbf{s}_2$ of Problem (6), $\mathbf{s}_1$ is said to dominate $\mathbf{s}_2$ if and only if

$$
\forall i \in 1, 2, \ldots k, f_i(\mathbf{s}_1) \leq f_i(\mathbf{s}_2),
$$

$$
and \ \exists j \in 1, 2, \ldots k, \ f_j(\mathbf{s}_1) < f_j(\mathbf{s}_2).
$$

The Pareto optimal set is constituted of feasible solutions not dominated by any other solutions, and the corresponding objective vectors of Pareto set form Pareto Front (PF). Multi-objective evolutionary algorithms (MOEAs) are designed to find a collection of optimal trade-off solutions so as to approximate Pareto Front. In

MOEA, commonly a set of solutions evolve altogether in each generation via crossover, mutation and non-dominated based selection.

B. Multi-objective Group Sparse Unmixing Model

The endmember bundle based sparse unmixing problem is translated into a bi-objective optimization problem and addressed by the designed algorithm. Considering the prior grouping information, we design the bi-objective minimization of reconstruction error and group sparsity as follows:

$$\min_{\mathbf{s}\in\{0,1\}^r} F(\mathbf{s}) = [f_1(\mathbf{s}), f_2(\mathbf{s})]^T$$

$$f_1(\mathbf{s}) = \begin{cases} \| \mathbf{Y} - \mathbf{A_s}\mathbf{X_s} \|_{\mathrm{F}}, & 0 \leq \| \mathbf{s} \|_0 \leq 2k \\ \\ \infty, & else \end{cases} \tag{7}$$

$$f_2(\mathbf{s}) = \big| \| \mathbf{s} \|_{G,0,q} - k \big|$$

In this article, we take spatial information into consideration via a uniform endmember selection among all pixels in the image. $\mathbf{s} \in \{0,1\}^m$ is a binary vector denoting endmember selection from spectral library with m spectra, in which $\mathbf{s}_i = 1$ means the i-th material in the library exists in the image $\mathbf{Y}$, and 0 otherwise. $f_1(\mathbf{s})$ is the reconstruction error of the observed image and is set finite only when the endmember selection satisfies the physical meaning of sparsity. In accordance with Ref. [28], we adopt the same algorithm HySime [44] to estimate the number of endmembers k aforehand, which accounts for an indicator in reconstruction error evaluation and an expectation of sparsity. The usage of estimated endmember numbers is a common tactic [28] to constrain the sparsity around a computed positive integer instead of 0 for accuracy. $\mathbf{A_s}$ is the corresponding subset of library $\mathbf{A}$ whose indices are denoted by the nonzero elements in $\mathbf{s}$, and $\mathbf{X_s}$ is the inverse abundance matrix of the new library $\mathbf{A_s}$ calculated from nonnegative least squares algorithm:

$$\mathbf{A_s} = \mathbf{A} \cdot \mathbf{s},$$

$$\mathbf{X_s} = \underset{\mathbf{X} \geq 0}{argmin} \| \mathbf{Y} - \mathbf{A_s}\mathbf{X} \|_{\mathrm{F}}.$$

$f_2(\mathbf{s})$ is a mixed norm integrating grouping structure of the spectral library, where $0 < q < 1$:

$$f_2(\mathbf{s}) = \big(\sum_{i=1}^{|G|} \| \mathbf{s}_{G_i} \|_0^q \big)^{\frac{1}{q}}$$

$\mathcal{L}_{G,0,q}$ quasi-norm better expresses both inter-group and intra-group sparsity than the regular $\mathcal{L}_0$-norm, enforcing sparsity on the endmember selection within bundle as well as bundles per se. Such expression manifests it is the number of materials instead of the spectra that is sparse in a pixel, meanwhile presenting the ascending sparsity within each bundle where only one endmember is supposed to exist.

$f_1(\mathbf{s})$ stands for the reconstruction error, and the quasi-norm denoted by $f_2(\mathbf{s})$ forms the group sparsity constraint. The two optimization objectives together compose the demands of sparse unmixing tasks. By optimizing Equation (7), trade-off solutions could be obtained to balance between accuracy and sparsity.

C. Optimization

In order to handle the nonconvex discrete optimization caused by the $\mathcal{L}_{G,0,q}$ norm, we propose a multi-objective evolutionary sparse unmixing method tailored for spectral library with group structure. We apply HySime on image data for endmember number estimation in advance, and k-means on spectral angle distance among the spectral library to form the group structure. Note that a predefined grouping structure is preferred, in which case the clustering step is not in need. As is demonstrated in pseudocode in Algorithm 1, the optimization procedure of the proposed MO-GSU adopts a framework similar to NSGA-II, in which the environmental selection via non-dominated sorting and crowding distance remains, yet an additional intra-group local search and a group oriented adaptive genetic operator are embedded for intra-group exploitation. The procedure of MO-GSU can be described as follows:

1) **Initialization**: First, we initialize a set of binary vectors with a sparse distribution as the initial population $\mathbf{P} = \{\mathbf{s}_1, \mathbf{s}_2, \ldots, \mathbf{s}_N\}$ with N individuals. 2) **Evolution**: In the first stage of evolutionary algorithm, the common NSGAII with the traditional one-point crossover and one-point flipping mutation operators is implemented. In the second stage, the overall population update procedure is exhibited in Figure 1 for each generation. Three sub-populations are generated to form the updated population: In the left branch of Figure 1, for sufficient local exploitation, an intra-group local search module designed for selection within bundle is conducted on a selected reference solution $\widetilde{\mathbf{s}}$ to generate population $\mathbf{P}_{\mathrm{LS}}$ as the first sub-population. In the middle branch of 1, the current population $\mathbf{P}$ is duplicated as the second sub-population. In the right branch of 1, a parent population $\mathbf{P}_{\mathrm{a}}$ consisting $2N$ individuals are selected via tournament selection from current population $\mathbf{P}$. Then N pairs of parent solutions are drawn without replacement to generate an offspring population $\mathbf{O}$ with the proposed group oriented adaptive genetic operator. The offspring population $\mathbf{O}$ with N individuals is the third sub-population. The combination of the three sub-populations $\mathbf{P}$, $\mathbf{O}$ and $\mathbf{P}_{\mathrm{LS}}$ are evaluated and sorted via non-dominated rank and crowding distance to form the updated population. The number of evaluations denotes the cumulative times of calculating the two objective functions. We use the number of evaluations as the stopping criterion to limit the computational cost under proper range. 3) **Optimal solution selection**: After meeting the stopping criterion, we return the current population as the proximate Pareto optimal set. We then select the most compatible solution for the unmixing task in consideration of the estimated endmember number and the knee point. Considering that neglected endmembers cause more inaccuracy than redundant ones, we first keep the solutions containing no less endmember than the estimated number, among which we choose the knee point as the final solution. 4) **Abundance inversion**: The final solution denotes the optimal endmember selection from the spectral library, the abundance matrix is then calculated accordingly using nonnegative least squares algorithm. In the next two sections, we detail the local search module and the group based genetic operator respectively.

D. Intra-group Local Search

MO-GSU synthesizes the genetic algorithm for its potential on global exploration and a novel intra-group local search strategy based on group structure for sufficient local exploitation. The local search strategy is performed in the second stage of the optimization, when in general the global exploration is accomplished.
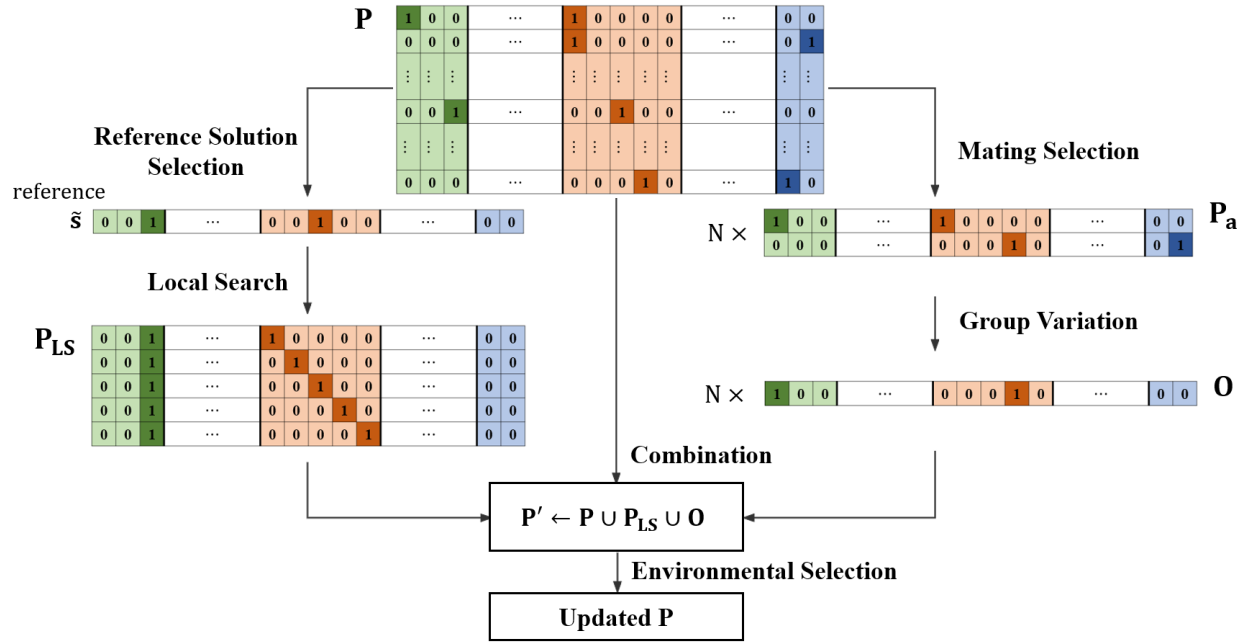
Fig. 1. The update procedure of each generation in the second stage. Each row of the current population **P** denotes a solution, different colors denote different groups of endmember, and the darkened colors denote the endmembers selected in the solution.

Algorithm 2 details the local search procedure which requires a local search population size N_{LS} so as to restrict complexity determined by the group size. A random solution $\widetilde{\mathbf{s}}$ is drawn from the non-dominated set of current population as the reference solution. A random group G_i is further drawn from the nonzero groups of $\widetilde{\mathbf{s}}$. Then a solution set $\mathbf{P}_{\mathrm{LS}}$ with up to N_{LS} solutions are generated, among which the elements in G_i varies while elsewhere are identical to the reference solution. Specifically, if the size of the chosen group G_i, $|G_i|$, is smaller than N_{LS}, the reference solution is duplicated for $|G_i|$ times. For the j-th duplicate, element of index G_{ij} is set as 1 and other indices in G_i as 0, where G_{ij} denotes the j-th index of group G_i. If $|G_i|$ is greater than N_{LS}, the operation holds except that the duplication is carried out for only N_{LS} times, and N_{LS} out of $|G_i|$ indices are randomly selected to construct N_{LS} solutions. Figure 2 provides a graphic demo of the local search module to select reference solution and random group, generating a local search population $\mathbf{P}_{\mathrm{LS}}$.

The local search module is proposed to compensate for the failure of evolutionary unmixing to locate the endmember within a bundle. Genetic algorithms determine the primary searching direction quickly due to its competence in global exploration, nevertheless the local exploitation suffers relatively. As a result, difficulty arises in the more delicate adjustment for the solutions during the optimization process. In the scenario of sparse unmixing on high correlation spectral library, multi-objective evolutionary approaches are able to narrow the selection of endmember down to bundle-wise. However the convergence speed tends to slow down when selecting one particular endmember from a group in the experiments. The local search module benefits endmember selection within bundle by conducting a more sufficient exploitation. In section 3.3, Figure 4 demonstrates how intra-group local search improves the endmember selection efficiency in experiment.

Algorithm 1 MO-GSU.

Input: $\mathbf{A}$(spectral library), $\mathbf{Y}$(image data), N(population size), n_{g}(group number).

Output: $\mathbf{s}$(endmember selection), $\mathbf{X_s}$(abundance).

1: **Initialization**:

2:   $k \leftarrow \mathrm{Hysime}(\mathbf{Y}, \mathbf{A})$;

3:   $G \leftarrow \mathrm{kmeans}(\mathbf{A}, n, \text{`SpectralAngleDistance'})$;

4:   $\mathbf{P} \leftarrow$ Initialize N binary individuals with sparsity;

5: **Evolution**:

6: **while** #evaluated $<$ #evaluation **do**

7:   $\mathbf{P}_{\mathrm{a}} \leftarrow$ Perform tournament selection on $\mathbf{P}$ for $2N$ times to select parent population of $2N$ individuals;

8:   **if** #evaluated $< 0.5\times$ #evaluation **then**

9:     **Stage I**:

10:     $\mathbf{O} \leftarrow$ Generate N offspring via one-point cross over and flipping mutation from $\mathbf{P}_{\mathrm{a}}$;

11:     $\mathbf{P} \leftarrow (\mathbf{P} \cup \mathbf{O})$;

12:   **else**

13:     **Stage II**:

14:     $\mathbf{O} \leftarrow GroupOperator(\mathbf{P}_{\mathrm{a}})$; //Generate N offspring via group based operator from $\mathbf{P}_{\mathrm{a}}$, see Algorithm 3

15:     $\mathbf{P}_{\mathrm{LS}} \leftarrow LocalSearch(\mathbf{P})$; //Generate $|G_i|$ individuals according to one random solution from $\mathbf{P}_{\mathrm{a}}$ and one random group G_i, see Algorithm 2

16:     $\mathbf{P}' \leftarrow (\mathbf{P} \cup \mathbf{P}_{\mathrm{LS}} \cup \mathbf{O})$;

17:   **end if**

18:   $\mathbf{P} \leftarrow$ Evaluate the $2N$ solution according to Equation (3), rank the individuals in $\mathbf{P}'$ by Pareto rank via non-dominated sorting and crowding distance, and update $\mathbf{P}$ with the first N individuals in $\mathbf{P}'$;

19: **end while**

20: **Abundance inversion**:

21: $\mathbf{s} \leftarrow$ Select the knee point from $\mathbf{P}$;

22: $\mathbf{X_s} \leftarrow$ Calculate the corresponding abundance according to Equation (7);

23: **return**: $\mathbf{s}, \mathbf{X_s}$;

E. Group Oriented Adaptive Genetic Operators

For the first stage of the evolutionary process, MO-GSU adopts the ordinary binary genetic operators namely one-point crossover and flipping mutation, and for the second we propose a new group-based variation with adaptive mutation probability. Algorithm 3 details the proposed variation. The crossover between two parent individuals is performed in groups uniformly. Elements in the same group are treated as a collective unit, and the units from two parents combines with each other at a given probability to reconstruct a new offspring. Instead of arbitrarily selecting a location and concatenate two segments from two parents, the group based crossover preserves the endmember
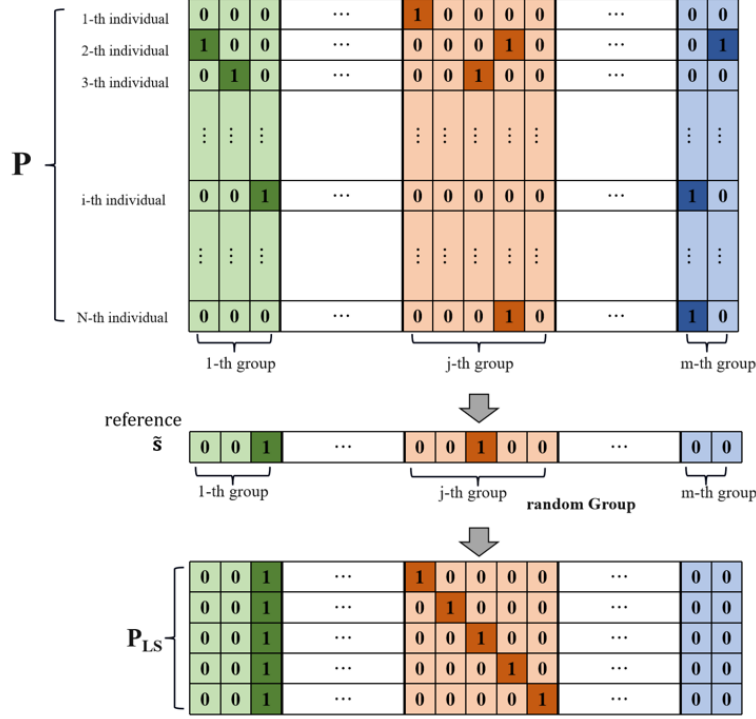
Fig. 2. The i-th individual is selected from the current population $\mathbf{P}$ and serves as the reference solution $\widetilde{\mathbf{s}}$. Randomly choose the j-th group which contains five variable. Duplicate the reference solution for five times and replace the j-th group with a five-by-five identity matrix.

selection within a bundle and reassemble bundles as a whole.

The mutation of an offspring is performed with an adaptive flipping probability to sustain the sparsity within group. For the nonzero groups G_i in the offspring solution $\mathbf{o}$, the adaptive probabilities in group G_i are given by Equation (8):

$$
\begin{cases}
p_1 = & \dfrac{d \times p + d_1 - 1}{2 \times d_1} \\[2mm]
p_0 = & \dfrac{d \times p - d_1 + 1}{2 \times (d - d_1)}
\end{cases}
\tag{8}
$$

where p_1 denotes the probability of an element flips from 1 to 0, and p_0 versa, d is the number of elements in group G_i, d_1 is the number of the current nonzero elements of solution $\mathbf{o}$ in group G_i, and p is the overall flipping probability.

Compared to the ordinary flipping mutation with the same overall flipping probability, the proposed mutation strategy sustains intra-group sparsity. The above formality satisfies the two conditions in Equation (9). The first condition is that the overall flipping probability equals to p, and the second is that the expected number of nonzero elements after mutation equals to d_1.

$$
\begin{cases}
d_1 \times p_1 + (d - d_1) \times p_0 = & d \times p \\[2mm]
d_1 \times (1 - p_1) + (d - d_1) \times p_0 = & d_1
\end{cases}
\tag{9}
$$

Algorithm 2 Local Search

Input: $\mathbf{P}$(current population), N_{LS}(local search population size).

Output: Output: $\mathbf{P}_{\text{LS}}$ (local search population).

1: $\widetilde{\mathbf{s}} \leftarrow$ Select a random solution from the non-dominated set of $\mathbf{P}$;

2: $G_i \leftarrow$ Select a random non-zero elements from $\widetilde{\mathbf{s}}$, set G_i as the corresponding group indices;

3: **if** $|G_i| \leq N_{\text{LS}}$ **then**

4:     $\mathbf{P}_{\text{LS}} \leftarrow$ Duplicate $\hat{\mathbf{s}}$ for $|G_i|$ times and form a population of size $|G_i|$;

5:     **for** $j = 1 : |G_i|$ **do**

6:         $\mathbf{P}_{\text{LS}}(j) \leftarrow$ adjust indices of group G_i for j-th solution in $\mathbf{P}_{\text{LS}}$: set the j-th index of G_i in j-th solution as 1, other indices of G_i in j-th solution as 0;

7:     **end for**

8: **else**

9:     $\mathbf{P}_{\text{LS}} \leftarrow$ Duplicate $\hat{\mathbf{s}}$ for N_{LS} times and form a population of size N_{LS};

10:     **for** $j = 1 : N_{\text{LS}}$ **do**

11:         $j' \leftarrow$ randomly select a non-repeated index between 1 and N_{LS};

12:         $\mathbf{P}_{\text{LS}}(j') \leftarrow$ adjust indices of group G_i for j-th solution in $\mathbf{P}_{\text{LS}}$: set the j'-th index of G_i in j-th solution as 1, other indices of G_i in j-th solution as 0;

13:     **end for**

14: **end if**

15: **return** $\mathbf{P}_{\text{LS}}$.

Such conditions illustrate that the overall flipping probability of the proposed mutation strategy is the same as general mutation operators. Nevertheless the number of the nonzero elements within group remains to be d_1 after the mutation. The adaptive flipping probability enhances the intra-group sparsity, consistent with the assumption of sparsity within bundle.

Considering the intra-group correlation and sparsity, genetic operators are supposed to transfer the position of the current nonzero element to another in the same group. Here, we give two theorems of the superiority of the proposed group operator to implement a more thorough exploitation over the classic one-point or uniform crossover and flipping mutation.

Theorem 1: For a nonzero group segment $\mathbf{g} = G_i$ and the Humming distance $H(\mathbf{g}, \mathbf{h})$ between two segments $\mathbf{g}, \mathbf{h}$, we have

$$P(H(\mathbf{g}, \mathbf{g}^{\text{am}}) = 2) > P(H(\mathbf{g}, \mathbf{g}^{\text{f}}) = 2),$$

where $\mathbf{g}^{\text{am}}$ denotes the group segment after adaptive mutation, and $\mathbf{g}^{\text{f}}$ denotes that after flipping mutation.

Proof 1: Due to the intra-group sparsity formed by the objective function, we assume there is no more than one

endmember in each bundle, i.e. $\|\mathbf{g}\|_0 = 1$. Under the above circumstance,

$$P(H(\mathbf{g}, \mathbf{g}^{\mathrm{am}}) = 2) = p_0 p_1 (1 - p_0)^{d-2}(d-1)$$

$$P(H(\mathbf{g}, \mathbf{g}^{\mathrm{um}}) = 2) = p^2 (1 - p)^{d-2}(d-1)$$

where d is the length of $\mathbf{g}$. According to the assumption, the d_1 in Equation (8) is substituted into 1. Therefore,

$$\frac{P(H(\mathbf{g}, \mathbf{g}^{\mathrm{am}}) = 2)}{P(H(\mathbf{g}, \mathbf{g}^{\mathrm{um}}) = 2)} = \Omega(d)$$

∎

Theorem 2: For the nonzero group segment $\mathbf{g} = G_i$ in individual $\mathbf{p}_1$, the segment $\mathbf{h}$ of the same group in individual $\mathbf{p}_2$ and the Humming distance $H(\mathbf{g}, \mathbf{h})$ between two segments, we have

$$q = P(H(\mathbf{g}, \mathbf{g}') = 2 \vee H(\mathbf{h}, \mathbf{h}') = 2 \mid H(\mathbf{g}, \mathbf{h}) < 2),$$

$$q^{\mathrm{g}} > q^{\mathrm{o}}, q^{\mathrm{g}} > q^{\mathrm{u}}$$

where $\mathbf{g}', \mathbf{h}'$ denote the segment after mutation and crossover, q denotes the probability of valid intra-group transfer after variation, and the superscripts represent different genetic operators. Specifically, g denotes the proposed group operator, o denotes flipping mutation and one-point crossover, o denotes flipping mutation and uniform crossover.

Proof 2: We follow the same assumption in Theorem 1, i.e. $\|\mathbf{g}\|_0 = 1$. For convenience, let

$$q_j \triangleq P(H(\mathbf{g}, \mathbf{g}') = 2 \vee H(\mathbf{h}, \mathbf{h}') = 2 \mid H(\mathbf{g}, \mathbf{h}) = j),$$

so $q = q_0 + q_1$.

$$q_0^{\mathrm{g}} = 2 p_0 p_1 (1 - p_0)^{d-2}(d-1) - [p_0 p_1 (1 - p_0)^{d-2}(d-1)]^2$$

$$q_0^{\mathrm{o}} = q_0^{\mathrm{u}} = 2 p^2 (1 - p)^{d-2}(d-1) - [p^2 (1 - p)^{d-2}(d-1)]^2$$

$$q_1^{\mathrm{g}} > p_0 p_1 (1 - p_0)^{d-2} + p(1 - p)^{d-1}$$

$$q_1^{\mathrm{o}} < p^2 (1 - p)^{d-2}(d-1) + p(1 - p)^{d-1}$$

where d is the length of $\mathbf{g}$. So,

$$\frac{q_0^{\mathrm{g}}}{q_0^{\mathrm{o}}} = \frac{q_0^{\mathrm{g}}}{q_0^{\mathrm{u}}} = \Omega(d), q_1^{\mathrm{g}} > q_1^{\mathrm{o}} = q_1^{\mathrm{u}}.$$

Hence,

$$q^{\mathrm{g}} > q^{\mathrm{o}} = q^{\mathrm{u}}.$$

∎

Remark: The ability of an operator to transfer one selected endmember to another of the same bundle is expressed via Hamming distance [45]. The Hamming distance of the group segments before and after variation equal to 2 accounts for a valid intra-group transfer, as in choosing a different endmember in the same group while remaining the intra-group sparsity. We evaluate operators by means of the valid transfer probability q, where a higher q accounts for an operator more effective. According to Theorem 1, the proposed group mutation operator with adaptive mutation probability is more likely to implement intra-group transfer than flipping mutation, which indicates that considering mutation alone, group based operator employs a more thorough exploitation. Theorem 2 evaluates the

combination of mutation and crossover operators. We come to the conclusion that group based operator performs more effectively than flipping mutation combined with one-point or uniform crossover.

Algorithm 3 Group Operator.

Input: $\mathbf{P}_a$ (parent population).

Output: $\mathbf{O}$ (offspring population).

  $\mathbf{O} \leftarrow \emptyset$;

  while $\mathbf{P}_a$ is not empty **do**

    Mating selection:

    $[\mathbf{pa}_1, \mathbf{pa}_2] \leftarrow$ Randomly select two solutions from $\mathbf{P}_a$;

    $\mathbf{P}_a \leftarrow \mathbf{P}_a \setminus [\mathbf{pa}_1, \mathbf{pa}_2]$;

    Crossover:

    $\mathbf{o} \leftarrow$ duplicate $\mathbf{pa}_1$;

    $\mathbf{o} \leftarrow$ adjust each group of $\mathbf{o}$: replace elements in group G_i of $\mathbf{o}$ with those of $\mathbf{pa}_2$ with a given probability uniformly;

    Mutation :

    $\mathbf{o} \leftarrow$ for the nonzero groups, do bit-wise flipping mutation with adaptive probability on each element of the nonzero group, and do flipping mutation with fixed probability on the other groups;

    $\mathbf{O} \leftarrow \mathbf{O} \cup \mathbf{o}$;

  end while

  return O

III. Experiments

In this section, the performance of MO-GSU is evaluated through experiments conducted on 3 synthetic data and 1 real data. It is compared with state-of-art sparse unmixing methods, bundle based and multi-objective methods.

The performance of unmixing accuracy is evaluated and quantified via the metric of signal-to-reconstruction error (SRE) defined as follow:

$$\text{SRE} = 10 \times \log \left(\frac{\text{E}(\| \mathbf{X}_{\text{real}} \|_F^2)}{\text{E}(\| \mathbf{X}_{\text{real}} - \mathbf{X} \|_F^2)} \right),$$

where $\mathbf{X}_{\text{real}}$ is the real abundance matrix and $\mathbf{X}$ is the estimated one. The larger value of SRE denotes the unmixing performance more effective.

Considering that MO-GSU is an endmember selection based method, we adopt the same evaluation parameter in [46] for selection accuracy assessment, namely true positive rate (TPR) and false positive rate (FPR). In the scenario of endmember selection, an endmember is positive if selected in the ground truth or the algorithm, and negative otherwise. In general, TPR and FPR are constrained between lower and upper bounds 0 and 1. The TPR equal to 1 and FPR equal to 0 implies a perfectly accurate selection in the algorithm, as in choosing the exact ground truth endmembers. Specifically, true positive (TP) denotes the number of positive and selected endmembers, false positive

(FP) denotes the number of negative and selected endmembers, true negative (TN) denotes the number of negative and unselected endmembers, false negative (FN) denotes the number of positive and unselected endmembers. TPR and FPR is thereby calculated as follow:

$$\text{TPR} = \frac{\text{TP}}{\text{TP} + \text{FN}}$$
$$\text{FPR} = \frac{\text{FP}}{\text{FP} + \text{TN}}$$

MO-GSU is compared with classic sparse unmixing methods, multi-objective based and grouping based methods: SUnSAL [17] relaxes the L_0 sparsity into L_1 norm and optimize abundances alternatively. Additionally a library pruning algorithm MUSIC [47] is executed ahead to alleviate the difficulty of high dimensionality down to size of 40. RSFoBa [48] is a greedy method for forward and backward selecting endmember simultaneously. SUnCNN [20] gains abundances via deep convolutional network. MOSU [27], SMOSU [28] and PMOSU [29] are three multi-objective unmixing approaches that transform the unmixing model into a multi-objective problem. MOSU adopts a classic non-dominance based algorithm NSGAII and SMOSU adopts a modified decomposition based algorithm MOEA/D for endmember selection respectively. PMOSU prunes the library via a gradual compression of search space and performs sparse regression in the same time. Methods presented in Ref. [38] incorporates structure of endmember bundles and present sparsity in mixed norm or double sparsity including three kinds of penalty: group, elitist, and fractional penalty, respectively corresponding to three quasinorms, $\mathcal{L}_{G,1,2}$, $\mathcal{L}_{G,2,1}$, and $\mathcal{L}_{G,1,q}$.

To verify the efficiency of MO-GSU for dealing with correlation in spectral library, different libraries of high correlation are used in the experiment. In Synthetic data 1 and Synthetic data 2, libraries of different degrees of correlation and grouping structures are first designed based on USGS library to simulate endmember bundles. In Synthetic data 3, a modified library containing 1543 spectra with complete reflectance of 224 bands is extracted from the USGS library, which also includes massive correlation. All the methods except SUnCNN are conducted using MATLAB R2018b on a desktop with Inter Core i5-8265U CPU @ 1.60 GHz 1.80 GHz of 8G memory running 64bit Windows operation system. SUnCNN is implemented in PyTorch framework running on NVIDIA GeForce RTX3060 Laptop GPU.

A. Synthetic Data 1

First, we generate 3 synthetic data sets from 3 designed high correlation spectral library with different degrees of correlation, which are constructed in the same way as [38], [49]. 20 spectra are randomly drawn from the United States Geological Survey (USGS) spectral library and used to form a library of size 400 including groups of high correlation spectral signals by simulating physical variations. USGS library contains thousands of spectral signals covering 224 bands. Specifically, 20 endmembers are randomly selected from the USGS library, respectively generating 20 spectra via different degrees of scaling variations and nonlinear quadratic perturbations as a simulation of variability induced by illumination and intrinsic factors. Hence, 3 prior libraries with increasing degrees of correlation and a naturally predetermined grouping structure is available, denoted as library 1, 2 and 3. Figure 3 illustrates the spectral library 3 built from the procedure mentioned above.

We generate a spatial-correlated abundance map via spatial low pass filter and restrict the abundance of each material no larger than 0.7 to increase unmixing difficulty. The image data to be unmixed is obtained by multiplying abundance map with randomly selected endmembers complying with the linear unmixing model, and a Gaussian white noise of 20 and 30db and is added to imitate sensor and measurement deviation.

The proposed MO-GSU is compared with the above mentioned methods, of which the ones marked asterisk denote an additional pruning process MUSIC ahead. The 3 methods from Ref. [10], namely approaches integrating group, elitist and fractional penalties. The three penalties respectively corresponds to sparsity regularization of the grouping based sparsity of $\mathcal{L}_{G,1,2}, \mathcal{L}_{G,2,1}$, and $\mathcal{L}_{G,1,q}$ norms. The objective function in MO-GSU adopts a similar sparsity to the fractional penalty. The parameters are set fixed instead of conducting a grid search. By contrast, the multi-objective evolutionary methods require no determination of parameter settings, which is convenient for practical use. MO-GSU is implemented on the basis of PlatEMO [50] with a novel algorithm and a homologous operator tailored for sparse unmixing with group structure proposed.
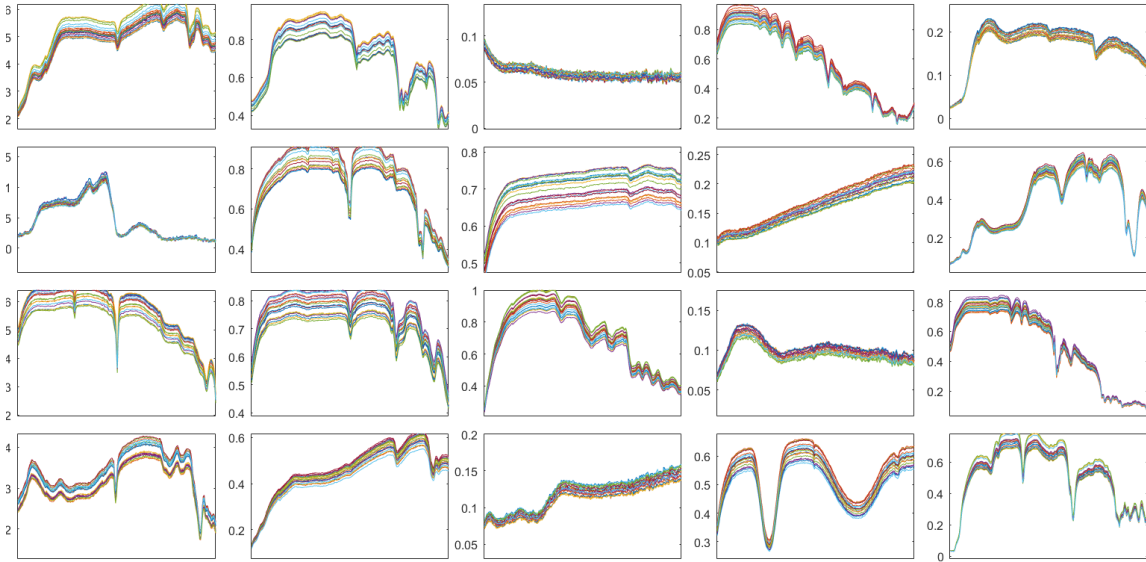
Fig. 3. The generated library of Synthetic Data 1. Each one of the 20 sub-figures is composed of 20 signatures variated from one selected endmember from the USGS library.

Table I shows the SRE results of conjoint endmembers on Synthetic Data 1 with 30 db noise and different degrees of correlation. Table I demonstrates that the proposed MO-GSU outperforms the classic and grouping based methods on the high-correlated spectral library in most cases, especially with higher degrees of correlation. Among the grouping based methods, the one incorporating fractional norm achieves better performances than elitist and group penalties. Accordingly, the effectiveness of the $\mathcal{L}_{G,1,q}$ norm is testified since the optimization approaches are alike. Compared to the $\mathcal{L}_{G,1,q}$ norm fractional penalty, the superiority gained by the inspired $\mathcal{L}_{G,0,q}$ norm based MO-GSU derives from the distinction of evolution optimization approach with group operators. In spite of the better performance MUSIC-SUnSAL obtain on 9 and 10 endmembers, MO-GSU operates on the original high correlation library with 10 times more spectra than the pruned and correlation eliminated library. When the

TABLE I

SRE RESULTS OF SYNTHETIC DATA 1, WHERE THE ASTERISK SUnSAL* AND RSFoBa* DENOTE CORRESPONDING METHODS COMBINED WITH THE PRUNING ALGORITHM MUSIC

Library	k	SUnSAL	SUnSAL*	RSFoBa*	SUnCNN	Group	Elitist	Fractional	MOSU	SMOSU	PMOSU	MO-GSU
1	3	11.92	13.40	4.56	4.86	0.44	0.28	8.21	**21.67**	**21.67**	**21.67**	**21.67**
	4	7.31	10.38	15.63	3.58	0.38	0.76	6.90	4.15	13.16	**21.95**	**21.95**
	5	12.60	14.19	5.91	5.23	0.52	0.22	11.56	14.37	**16.24**	**16.24**	**16.24**
	6	10.92	14.70	17.80	2.39	0.42	0.76	8.95	**17.80**	**17.80**	**17.80**	**17.80**
	7	11.66	15.46	15.52	1.74	0.42	1.02	10.06	15.42	**15.52**	**15.52**	**15.52**
	8	9.52	13.50	4.32	0.77	0.42	0.33	7.95	4.98	5.18	**13.87**	12.73
	9	10.75	**14.48**	8.66	1.05	0.44	0.16	7.73	8.02	5.63	13.52	13.52
	10	11.67	**15.72**	7.06	1.72	0.42	0.81	8.47	12.58	5.62	13.58	12.97
2	3	8.50	11.58	15.64	11.49	0.44	0.00	9.79	2.14	14.11	**32.19**	**32.19**
	4	10.85	14.15	18.14	7.29	0.45	0.26	9.98	**18.14**	**18.14**	**18.14**	**18.14**
	5	10.57	13.13	**17.29**	7.45	0.47	0.00	10.55	12.61	**17.29**	**17.29**	**17.29**
	6	6.20	10.16	5.63	4.30	0.40	1.02	5.79	11.12	9.39	**11.24**	**11.24**
	7	9.15	13.15	6.78	4.58	0.47	0.15	8.14	5.47	12.59	**15.06**	14.74
	8	7.26	6.87	6.82	2.70	0.40	0.76	6.90	4.57	6.12	7.55	**11.41**
	9	10.05	**13.92**	8.13	2.60	0.45	0.64	8.81	5.82	4.88	11.84	11.84
	10	9.72	**13.41**	7.86	2.32	0.45	0.28	9.12	8.17	3.51	10.56	10.56
3	3	6.27	7.15	5.56	12.15	0.63	0.11	8.19	**12.62**	**12.62**	**12.62**	**12.62**
	4	3.00	5.74	8.56	4.80	0.43	0.04	2.97	2.84	**23.34**	**23.34**	**23.34**
	5	5.08	9.33	1.72	6.83	0.42	0.20	4.61	1.78	**28.21**	**28.21**	**28.21**
	6	2.15	3.75	0.01	0.36	0.01	4.84	2.39	1.49	-	**7.30**	4.80
	7	3.28	8.47	5.88	4.49	0.37	0.05	2.99	3.54	**17.75**	8.02	**17.75**
	8	2.59	5.27	5.13	3.13	0.42	0.22	2.29	-	-	6.04	**19.00**
	9	3.02	10.32	8.53	2.69	0.37	0.33	3.02	1.13	**14.90**	10.17	**14.90**
	10	5.18	**12.37**	8.29	2.33	0.43	0.28	4.21	3.06	7.32	8.24	8.60

TABLE II

EXECUTION TIME(S) OF SYNTHETIC DATA 1

	Group	Elitist	Fractional	MOSU	SMOSU	PMOSU	MO-GSU
Time(s)	153(±5.5)	173(±5.8)	225(±6.8)	241(±9.5)	230(±6.7)	185.5(±4.0)	237.7(±16.5)

prior library is fixed to the original one, the SRE results of SUnSAL are diminished. Besides, the advantages brought by the pruning process tend to reduce when the correlation increases due to the possibility to prune the true endmembers. Table II displays the average execution time of MO-GSU as well as multi-objective and grouping based unmixing methods. The multi-objective methods are implemented with the fixed evaluation number of 20000 and the grouping methods with default settings. Compared to other multi-objective methods, the proposed MO-GSU can achieve better SRE results under limited time. Besides, the comparable time consuming indicates that the proposed local search and group oriented adaptive genetic operator module does not improve unmixing effect by consuming more computational time.

B. Synthetic Data 2

In order to testify the effectiveness of the proposed method on high correlation spectral library, we build three 2000 size libraries with different correlation level in the same way as Synthetic Data 1. In Synthetic Data 1, n_{group} randomly selected endmembers generate s_{group} spectra respectively, presenting n_{group} high correlation spectral groups with the size of s_{group}. Synthetic Data 2 constructs three libraries of the same size but employing different settings of $n_{\mathrm{group}}, s_{\mathrm{group}}$, which are (100,20), (40,50), and (20,100), enforcing an progressively enhancive correlation within each group. Synthetic Data 2 generates abundance map based on Dirichlet distribution which is compatible with ANC, ASC constraints and bears no spatial correlation.

Table III shows the TPR, FPR and the SRE results of endmember selection of different combination of three levels, namely noise, endmember number and library correlation. The selection accuracy of MO-GSU on large scale spectral library is validated attributing to most TPR and FPR values equal 1 and 0, which is an indication of perfectly accurate selection. In general, the selection difficulty increases in response to the growth of endmember numbers and noises. Three spectral libraries with progressively strong correlation examine the capacity of MO-GSU for intra-group selection. As in Table III, MO-GSU reaches perfect selection in most cases.

From Table III, the effectiveness of MO-GSU suffers with a larger number of groups, seemingly a negative outcome. Note that such outcome is more likely the aftermath of the inevitable drawback of multi-objective unmixing assessing criteria rather than MO-GSU's inability of extremely complicated combination. For instance, in the experiment on 20db noise, 10 endmembers and group parameter $(n_{\mathrm{group}}, s_{\mathrm{group}}) = (40, 50)$, the TPR and FPR of the final solution provided by MO-GSU is 0.90 and 5.03×10^{-4}. In this case, the failure of the proposed algorithm to correct selection is a systematic drawback, since the objective vector of MO-GSU's solution is $(48.0344, 10)$ and of the correct selection is $(48.0346, 10)$. Therefore in Pareto-dominant wise, MO-GSU's solution is a better solution than the correct selection. Hence it can be safely inferred that the correct selection has been visited yet discarded in the evolutionary process.

C. Synthetic Data 3

USGS library stores spectral signal data with group structure naturally formulated by bundles of multiple endmembers per material. Hence, it is naturally a high correlation library with endmembers varying in shape and different degrees of correlation. Synthetic Data 3 conducts abundance and image data generation on a subset

TABLE III

TPR,FPR AND SRE RESULTS ON SYNTHETIC DATA 2 OF DIFFERENT NOISES, ENDMEMBER NUMBERS, AND CORRELATION.

SNR	k	(100,20)			(40,50)			(20,100)		
		TPR	FPR	SRE	TPR	FPR	SRE	TPR	FPR	SRE
20db	3	1	0	19.40	1	0	18.15	1	0	9.44
	4	0.75	5.01×10^{-4}	3.99	1	0	16.29	1	0	16.08
	5	1	0	14.69	1	0	16.81	1	0	13.74
	6	1	0	11.88	1	0	12.89	1	0	4.06
	7	1	0	9.80	1	0	9.26	1	0	3.51
	8	0.63	1.51×10^{-3}	1.63	0.63	1.00×10^{-3}	1.03	0.75	1.00e-3	1.89
	9	0.89	5.02×10^{-4}	4.11	0.89	5.02×10^{-4}	5.48	0.89	5.02×10^{-4}	2.85
	10	0.8	1.00×10^{-3}	4.21	0.90	5.03×10^{-4}	4.41	0.60	1.01×10^{-4}	1.02
30db	3	1	0	29.84	1	0	28.05	1	0	32.78
	4	1	0	14.38	1	0	23.22	1	0	23.92
	5	1	0	20.96	1	0	28.16	1	0	22.80
	6	0.83	5.02×10^{-4}	4.45	1	0	17.09	1	0	19.08
	7	1	0	14.47	1	0	21.64	1	0	18.87
	8	0.88	5.02×10^{-4}	8.30	1	0	13.35	1	0	19.25
	9	1	0	11.77	1	0	12.59	1	0	12.28
	10	0.90	5.03×10^{-4}	5.31	1	0	14.72	1	0	15.41
40db	3	1	0	36.70	1	0	36.17	1	0	47.85
	4	1	0	39.94	1	0	31.71	1	0	36.86
	5	1	0	29.35	1	0	29.26	1	0	33.18
	6	1	0	26.09	1	0	26.11	1	0	33.21
	7	1	0	20.78	1	0	26.34	1	0	29.69
	8	1	0	13.09	1	0	18.58	0.88	5.02×10^{-4}	7.14
	9	1	0	24.01	1	0	24.16	0.89	0	9.58
	10	1	0	24.25	1	0	17.02	0.90	0	10.83

of the USGS spectral library version seven (Splib07). Some spectra from the original USGS library have different bands of data missing from the 224 bands, which are excluded from the prior library. The modified spectral library contains 1543 endmembers with complete reflectance of 224 bands. Synthetic Data 3 adopts the same abundance and image generation methods as Synthetic Data 1, while the spectral libraries vary.

Figure 4 is a demonstration of how endmember selection evolves in MOSU and MO-GSU. Figure 4 depicts that classic genetic algorithm is capable of locating the right group efficiently, yet ineffective to adjust intra-group selection for a long time. On the contrary, after a certain amount of regular evolution by NSGAII, MO-GSU is more
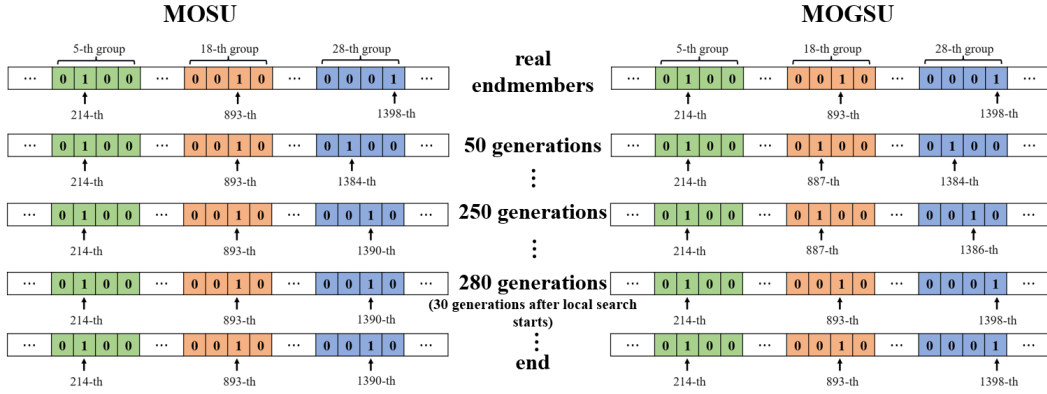
Fig. 4. The evolutionary process of MOSU and MO-GSU. From top to bottom are the real endmember indices and the selection endmember of different evolutionary generations.
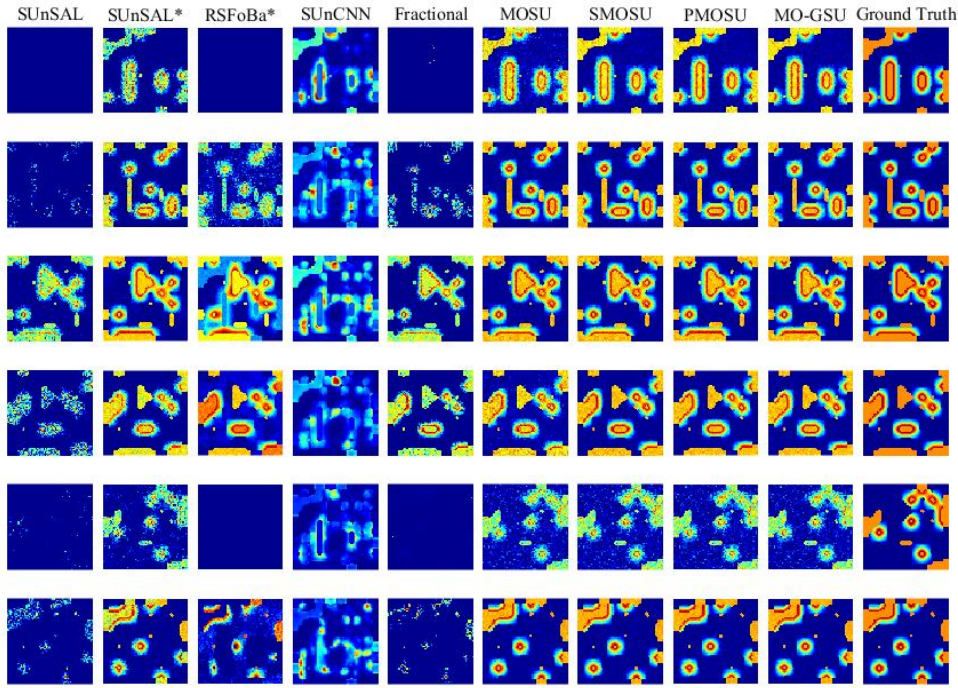

Fig. 5. Estimated and Real Abundance Maps of Synthetic Data 3. Each row represents a material, and each column represents a method.

flexible and approximates both the correct group and the endmember within, showing a promising potential. Figure 5 is a graphic illustration of abundance maps generated from the above methods on the image of 6 endmembers and 30db noise. Some sub-graphs are pure dark, meaning the corresponding endmember not chosen by the algorithm. Compared with the abundance from other methods, MO-GSU generates a figure of sharper edge, more similar to that of the ground truth. Figure 5 visually examines the effectiveness of MO-GSU by a more accurate outcome.

Table IV shows the SRE results of conjoint endmembers on Synthetic Data 3 with various noises. The results under both the more realistic circumstance of 40db and the more difficult circumstances with 20db and 30db are

TABLE IV

SRE RESULTS OF SYNTHETIC DATA 3, WHERE THE ASTERISK * IN SUNSAL*, SMP*, CLSUNSAL* ,SMOSU* DENOTES ALGORITHMS
COMBINED WITH THE PRUNING ALGORITHM MUSIC

Noise	Number	SUnSAL	SUnSAL*	RSFoBa*	SUnCNN	Fractional	MOSU	SMOSU	PMOSU	MO-GSU
20db	3	1.98	11.44	2.65	7.38	1.93	18.58	12.35	**22.91**	**22.91**
	4	1.62	4.73	4.24	1.93	0.65	5.86	3.88	5.20	**7.91**
	5	2.96	10.17	-	3.67	3.26	0.60	-	**16.83**	**16.83**
	6	0.63	2.29	3.21	0.42	-	-0.43	-	3.09	**6.74**
	7	0.14	2.04	5.35	0.40	-	-	-	-	3.20
	8	0.56	0.74	5.67	0.73	-	1.69	-	2.17	2.50
	9	0.47	3.31	5.77	0.71	-0.15	-	-	2.29	**5.90**
	10	1.27	1.99	6.92	1.07	0.18	2.13	-	1.90	3.63
30db	3	2.26	4.69	4.77	1.30	0.59	1.62	**11.82**	**11.82**	**11.82**
	4	0.70	2.97	4.48	1.14	1.31	-	5.58	5.89	**6.98**
	5	3.28	8.52	4.98	3.39	1.91	23.25	**28.28**	**28.28**	3.96
	6	1.61	10.95	2.46	1.01	0.03	14.13	**15.45**	**15.45**	**15.45**
	7	3.37	10.48	6.15	1.71	2.70	17.09	**21.45**	**21.45**	8.18
	8	1.58	5.47	7.27	0.89	-0.72	1.40	6.95	7.43	**8.52**
	9	2.24	**6.85**	6.70	0.94	0.82	4.43	5.70	6.08	6.14
	10	1.03	4.13	-	0.87	0.82	5.13	3.69	7.27	**7.92**
40db	3	3.75	15.70	18.92	9.25	9.52	-0.85	**38.82**	**38.82**	**38.82**
	4	3.47	8.26	2.49	10.02	3.80	0.00	**33.77**	**33.77**	**33.77**
	5	1.19	12.85	5.20	0.69	0.09	**21.77**	**21.77**	**21.77**	**21.77**
	6	5.47	18.45	5.45	2.65	3.24	5.34	**28.38**	**28.38**	2.20
	7	4.80	15.35	6.22	1.29	2.60	8.19	6.71	**23.02**	**23.02**
	8	0.90	6.16	0.42	0.55	1.09	1.98	5.12	-	**8.90**
	9	4.88	**15.46**	4.56	1.51	4.21	-0.07	7.98	5.02	5.81
	10	0.90	6.16	0.42	0.30	1.09	3.65	2.65	-	**8.90**

presented. Table IV demonstrates that the proposed method is still valid when the group structure of the library is not predefined but gained by clustering method. We choose fractional penalty as the representative of bundle-based methods, since the sparsity regularization form is the same as MO-GSU. MO-GSU is compared to multi-objective methods with the same amount of evaluations and population size. MO-GSU is conducted on the original prior library of 1543 spectra, while some of the comparison methods perform on the pruned library of size 40. MO-GSU outperforms the rest methods in most cases. MOSU shows potential when there are more true endmembers, which implies a better exploration than MO-GSU given limited evaluations. The incompetence of perfectly accurate

selection when MO-GSU faces endmember number increasing speaks the unbalance between local and global search. In particular, the convergence of local search within group outweighs global variation among groups immediately after the local search module starts and consequently the recombination of groups is harder. Such problem may be relieved by setting the starting point of local search adaptive according to estimated endmember numbers. More specifically, the starting point of the second stage is proportional to the endmember number to guarantee a more thorough exploration.

D. Real Data
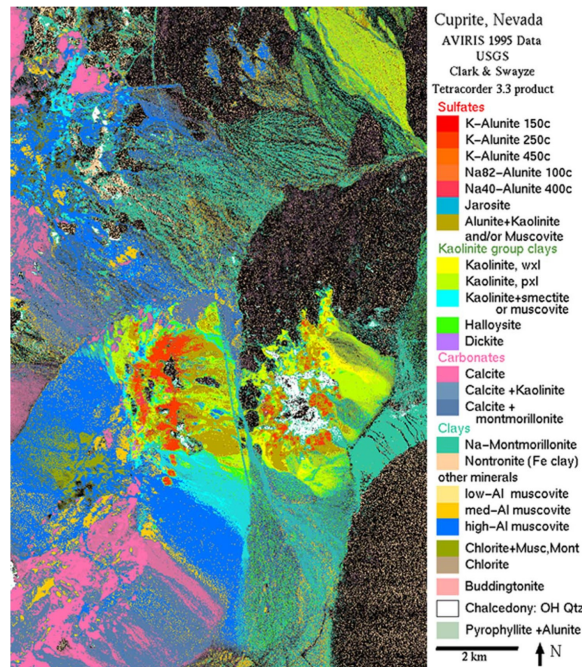
Fig. 6. Mineral map of Cuprite dataset.

We choose Cuprite data acquired by AVIRIS with the size of 250×190 pixels for real data experiment. The original image comprises 224 bands ranging from 370 nm to 2480 nm. From the 224 bands, a few noisy and water absorption ones are discarded and the final image size is $250 \times 190 \times 188$. The library is the first chapter of splib06a with 498 endmembers, including the signatures of the above mentioned materials and the noisy bands in the spectral library are removed accordingly.

Figure 6 provides a qualitive reference of the groundtruth materials. Note that each pixel in Figure 6 is assigned to a single material. Figure 7 illustrates the abundance maps of Alunite, Jarosite, Kaolin+Smectite, Buddingtonite and Chalcedony from the top down obtained by sparse unmixing methods. In practice, the quantitative criteria of the groundtruth are hard to achieve. The sub-images of Figure 7 provide a qualitative and visualized assessment of the effectiveness of proposed method. Compared to Figure 6, MO-GSU is able to select endmembers more accurately and achieves a clearer outline reflecting structural information, so that the performance on real world application is
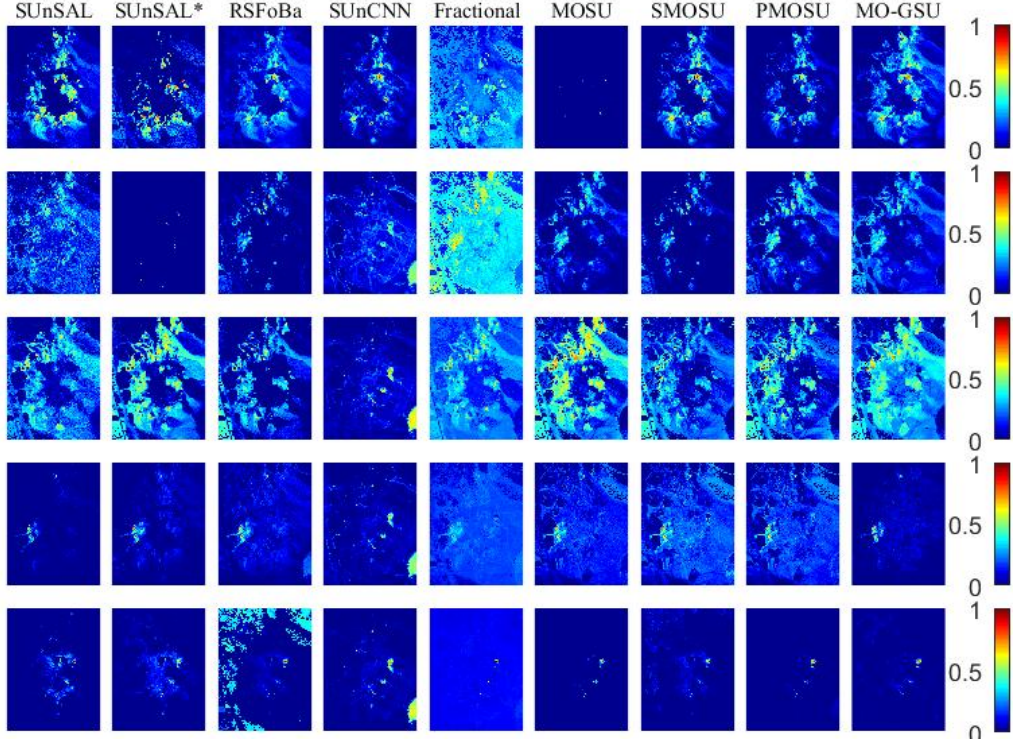
Fig. 7. Estimated maps of real data. From top to bottom, each row represents a material, namely Alunite, Jarosite, Kaolin+Smectite, Buddingtonite and Chalcedony, and each column represents a method.

testified. Some abundance maps of the grouping method with fractional norm appears average distribution among pixels, which indicates some noise may be introduced into the abundance map.

IV. CONCLUSIONS

In this paper, we propose a multi-objective sparse unmixing method based on group structure. The high correlation within endmember bundle formulates a group structure inside spectral library. Inspired by the fractional sparsity penalty represented by mixed norm, the proposed MO-GSU replace the $\mathcal{L}_0$ sparsity from classic multi-objective sparse unmixing methods with a $\mathcal{L}_{0,q}$ norm involving group structure G. In order to minimize the reconstruction error of the image and the $\mathcal{L}_{0,q}$ norm sparsity, we adopt the framework of NSGAII. For the purpose of accurate endmember identification within each group, an intra-group local search strategy is proposed to exploit intra group selection. We design a group oriented adaptive genetic operator to further ensure the balance between inter-group exploration and intra-group exploitation. We provide theoretical proof for the proposed group operator of a more sufficient intra-group endmember exploitation. Experimental results on synthetic and real data show that the proposed method is valid for strong correlation spectral libraries. The main shortcoming of evolutionary algorithms lies in the great time consumption and incompetence for guaranteed convergence, especially facing the ever-expanding spectral library. In the future, we would mainly focus on speeding up convergence by introducing gradient based orientation, as well as adjusting multi-gradient descend to solve unmixing problem.

REFERENCES

[1] N. Keshava and J. F. Mustard, "Spectral unmixing," *IEEE signal processing magazine*, vol. 19, no. 1, pp. 44–57, 2002.

[2] Y. Yuan, Z. Zhang, and Q. Wang, "Improved collaborative non-negative matrix factorization and total variation for hyperspectral unmixing," *IEEE Journal of Selected Topics in Applied Earth Observations and Remote Sensing*, vol. 13, pp. 998–1010, 2020.

[3] X. Tao, M. E. Paoletti, J. M. Haut, L. Han, P. Ren, J. Plaza, and A. Plaza, "Endmember estimation from hyperspectral images using geometric distances," *IEEE Geoscience and Remote Sensing Letters*, vol. 19, pp. 1–5, 2021.

[4] J. Yuan, Y. Zhang, and F. Gao, "An overview on linear hyperspectral unmixing," *J. Infrared Millim. Waves*, vol. 37, no. 5, pp. 553–571, 2018.

[5] N. Dobigeon, J.-Y. Tourneret, C. Richard, J. C. M. Bermudez, S. McLaughlin, and A. O. Hero, "Nonlinear unmixing of hyperspectral images: Models and algorithms," *IEEE Signal processing magazine*, vol. 31, no. 1, pp. 82–94, 2013.

[6] R. Heylen, M. Parente, and P. Gader, "A review of nonlinear hyperspectral unmixing methods," *IEEE Journal of Selected Topics in Applied Earth Observations and Remote Sensing*, vol. 7, no. 6, pp. 1844–1868, 2014.

[7] A. M. S. Ang and N. Gillis, "Algorithms and comparisons of nonnegative matrix factorizations with volume regularization for hyperspectral unmixing," *IEEE Journal of Selected Topics in Applied Earth Observations and Remote Sensing*, vol. 12, no. 12, pp. 4843–4853, 2019.

[8] S. Das, A. Routray, and A. K. Deb, "Convex set based abundance constrained unmixing of hyperspectral image," in *2017 14th IEEE India Council International Conference (INDICON)*. IEEE, 2017, pp. 1–5.

[9] S. Zhang, A. Agathos, and J. Li, "Robust minimum volume simplex analysis for hyperspectral unmixing," *IEEE Transactions on Geoscience and Remote Sensing*, vol. 55, no. 11, pp. 6431–6439, 2017.

[10] L. Drumetz, J. Chanussot, C. Jutten, W.-K. Ma, and A. Iwasaki, "Spectral variability aware blind hyperspectral image unmixing based on convex geometry," *IEEE Transactions on Image Processing*, vol. 29, pp. 4568–4582, 2020.

[11] N. Dobigeon, S. Moussaoui, M. Coulon, J.-Y. Tourneret, and A. O. Hero, "Joint bayesian endmember extraction and linear unmixing for hyperspectral imagery," *IEEE Transactions on Signal Processing*, vol. 57, no. 11, pp. 4355–4368, 2009.

[12] K. E. Themelis, A. A. Rontogiannis, and K. D. Koutroumbas, "A novel hierarchical bayesian approach for sparse semisupervised hyperspectral unmixing," *IEEE Transactions on Signal Processing*, vol. 60, no. 2, pp. 585–599, 2011.

[13] S. Jia and Y. Qian, "Constrained nonnegative matrix factorization for hyperspectral unmixing," *IEEE Transactions on Geoscience and Remote Sensing*, vol. 47, no. 1, pp. 161–173, 2008.

[14] W. He, H. Zhang, and L. Zhang, "Total variation regularized reweighted sparse nonnegative matrix factorization for hyperspectral unmixing," *IEEE Transactions on Geoscience and Remote Sensing*, vol. 55, no. 7, pp. 3909–3921, 2017.

[15] C.-H. Lin, F. Ma, C.-Y. Chi, and C.-H. Hsieh, "A convex optimization-based coupled nonnegative matrix factorization algorithm for hyperspectral and multispectral data fusion," *IEEE Transactions on Geoscience and Remote Sensing*, vol. 56, no. 3, pp. 1652–1667, 2017.

[16] W. Tang, Z. Shi, Y. Wu, and C. Zhang, "Sparse unmixing of hyperspectral data using spectral a priori information," *IEEE Transactions on Geoscience and Remote Sensing*, vol. 53, no. 2, pp. 770–783, 2014.

[17] M.-D. Iordache, J. M. Bioucas-Dias, and A. Plaza, "Sparse unmixing of hyperspectral data," *IEEE Transactions on Geoscience and Remote Sensing*, vol. 49, no. 6, pp. 2014–2039, 2011.

[18] L. Sun, Z. Wu, L. Xiao, J. Liu, Z. Wei, and F. Dang, "A novel l 1/2 sparse regression method for hyperspectral unmixing," *International journal of remote sensing*, vol. 34, no. 20, pp. 6983–7001, 2013.

[19] F. Chen and Y. Zhang, "Sparse hyperspectral unmixing based on constrained lp-l 2 optimization," *IEEE Geoscience and Remote Sensing Letters*, vol. 10, no. 5, pp. 1142–1146, 2013.

[20] B. Rasti and B. Koirala, "Suncnn: Sparse unmixing using unsupervised convolutional neural network," *IEEE Geoscience and Remote Sensing Letters*, vol. 19, pp. 1–5, 2021.

[21] A. Messac, G. J. Sundararaj, R. V. Tappeta, and J. E. Renaud, "Ability of objective functions to generate points on nonconvex pareto frontiers," *AIAA journal*, vol. 38, no. 6, pp. 1084–1091, 2000.

[22] C. Li, Y. Liu, J. Cheng, R. Song, J. Ma, C. Sui, and X. Chen, "Sparse unmixing of hyperspectral data with bandwise model," *Information sciences*, vol. 512, pp. 1424–1441, 2020.

[23] M. Song, Y. Zhong, A. Ma, X. Xu, and L. Zhang, "A joint spectral unmixing and subpixel mapping framework based on multiobjective optimization," *IEEE Transactions on Geoscience and Remote Sensing*, 2021.

[24] L. Tong, B. Du, R. Liu, and L. Zhang, "An improved multiobjective discrete particle swarm optimization for hyperspectral endmember extraction," *IEEE Transactions on Geoscience and Remote Sensing*, vol. 57, no. 10, pp. 7872–7882, 2019.

[25] X. Jiang, M. Gong, T. Zhan, and M. Zhang, "Multiobjective endmember extraction based on bilinear mixture model," *IEEE Transactions on Geoscience and Remote Sensing*, vol. 58, no. 11, pp. 8192–8210, 2020.

[26] R. Liu and X. Zhu, "Endmember bundle extraction based on multiobjective optimization," *IEEE Transactions on Geoscience and Remote Sensing*, vol. 59, no. 10, pp. 8630–8645, 2020.

[27] M. Gong, H. Li, E. Luo, J. Liu, and J. Liu, "A multiobjective cooperative coevolutionary algorithm for hyperspectral sparse unmixing," *IEEE transactions on evolutionary computation*, vol. 21, no. 2, pp. 234–248, 2016.

[28] X. Xu, Z. Shi, and B. Pan, "l0-based sparse hyperspectral unmixing using spectral information and a multi-objectives formulation," *ISPRS journal of photogrammetry and remote sensing*, vol. 141, pp. 46–58, 2018.

[29] X. Xu, B. Pan, Z. Chen, Z. Shi, and T. Li, "Simultaneously multiobjective sparse unmixing and library pruning for hyperspectral imagery," *IEEE Transactions on Geoscience and Remote Sensing*, vol. 59, no. 4, pp. 3383–3395, 2020.

[30] X. Jiang, M. Gong, T. Zhan, K. Sheng, and M. Xu, "Efficient two-phase multiobjective sparse unmixing approach for hyperspectral data," *IEEE Journal of Selected Topics in Applied Earth Observations and Remote Sensing*, vol. 14, pp. 2418–2431, 2021.

[31] S. Liu, Q. Lin, K.-C. Wong, Q. Li, and K. C. Tan, "Evolutionary large-scale multiobjective optimization: Benchmarks and algorithms," *IEEE Transactions on Evolutionary Computation*, 2021.

[32] B. Somers, G. P. Asner, L. Tits, and P. Coppin, "Endmember variability in spectral mixture analysis: A review," *Remote Sensing of Environment*, vol. 115, no. 7, pp. 1603–1616, 2011.

[33] Y. Zhou, A. Rangarajan, and P. D. Gader, "A gaussian mixture model representation of endmember variability in hyperspectral unmixing," *IEEE Transactions on Image Processing*, vol. 27, no. 5, pp. 2242–2256, 2018.

[34] J. Yu, B. Wang, Y. Lin, F. Li, and J. Cai, "A novel inequality-constrained weighted linear mixture model for endmember variability," *Remote Sensing of Environment*, vol. 257, p. 112359, 2021.

[35] C. A. Bateson, G. P. Asner, and C. A. Wessman, "Endmember bundles: A new approach to incorporating endmember variability into spectral mixture analysis," *IEEE transactions on geoscience and remote sensing*, vol. 38, no. 2, pp. 1083–1094, 2000.

[36] T. Uezato, M. Fauvel, and N. Dobigeon, "Hyperspectral unmixing with spectral variability using adaptive bundles and double sparsity," *IEEE Transactions on Geoscience and Remote Sensing*, vol. 57, no. 6, pp. 3980–3992, 2019.

[37] S. G. Azar, S. Meshgini, S. Beheshti, and T. Y. Rezaii, "Linear mixing model with scaled bundle dictionary for hyperspectral unmixing with spectral variability," *Signal Processing*, vol. 188, p. 108214, 2021.

[38] L. Drumetz, T. R. Meyer, J. Chanussot, A. L. Bertozzi, and C. Jutten, "Hyperspectral image unmixing with endmember bundles and group sparsity inducing mixed norms," *IEEE Transactions on Image Processing*, vol. 28, no. 7, pp. 3435–3450, 2019.

[39] J. Parsa, M. Sadeghi, M. Babaie-Zadeh, and C. Jutten, "Joint low mutual and average coherence dictionary learning," in *2018 26th European Signal Processing Conference (EUSIPCO)*.   IEEE, 2018, pp. 1725–1729.

[40] S. Das, A. Routray, and A. K. Deb, "Fast semi-supervised unmixing of hyperspectral image by mutual coherence reduction and recursive pca," *Remote Sensing*, vol. 10, no. 7, p. 1106, 2018.

[41] K. Sindhya, K. Deb, and K. Miettinen, "A local search based evolutionary multi-objective optimization approach for fast and accurate convergence," in *International Conference on Parallel Problem Solving from Nature*.   Springer, 2008, pp. 815–824.

[42] A.-D. Li, B. Xue, and M. Zhang, "Multi-objective feature selection using hybridization of a genetic algorithm and direct multisearch for key quality characteristic selection," *Information Sciences*, vol. 523, pp. 245–265, 2020.

[43] E. Osaba, J. Del Ser, C. Cotta, and P. Moscato, "Memetic computing: Accelerating optimization heuristics with problem-dependent local search methods," p. 101047, 2022.

[44] J. M. Bioucas-Dias and J. M. Nascimento, "Hyperspectral subspace identification," *IEEE Transactions on Geoscience and Remote Sensing*, vol. 46, no. 8, pp. 2435–2445, 2008.

[45] C. Qian, C. Bian, and C. Feng, "Subset selection by pareto optimization with recombination," in *Proceedings of the AAAI Conference on Artificial Intelligence*, vol. 34, no. 03, 2020, pp. 2408–2415.

[46] X. Xu, Z. Shi, B. Pan, and X. Li, "A classification-based model for multi-objective hyperspectral sparse unmixing," *IEEE Transactions on Geoscience and Remote Sensing*, vol. 57, no. 12, pp. 9612–9625, 2019.

[47] M.-D. Iordache, J. M. Bioucas-Dias, A. Plaza, and B. Somers, "Music-csr: Hyperspectral unmixing via multiple signal classification and collaborative sparse regression," *IEEE Transactions on Geoscience and Remote Sensing*, vol. 52, no. 7, pp. 4364–4382, 2013.

[48] W. Tang, Z. Shi, and Y. Wu, "Regularized simultaneous forward–backward greedy algorithm for sparse unmixing of hyperspectral data," *IEEE Transactions on Geoscience and Remote Sensing*, vol. 52, no. 9, pp. 5271–5288, 2013.

[49] L. Drumetz, M.-A. Veganzones, S. Henrot, R. Phlypo, J. Chanussot, and C. Jutten, "Blind hyperspectral unmixing using an extended linear mixing model to address spectral variability," *IEEE Transactions on Image Processing*, vol. 25, no. 8, pp. 3890–3905, 2016.

[50] Y. Tian, R. Cheng, X. Zhang, and Y. Jin, "Platemo: A matlab platform for evolutionary multi-objective optimization [educational forum]," *IEEE Computational Intelligence Magazine*, vol. 12, no. 4, pp. 73–87, 2017.